doi.org/10.1002/cbdv.202301824 Research Article CHEMISTRY & BIODIVERSITY

www.cb.wiley.com

Design and Synthesis of Pyrazole Carboxamide Derivatives as Selective Cholinesterase and Carbonic Anhydrase Inhibitors: Molecular Docking and Biological Evaluation

Mustafa Durgun,*[a] Suleyman Akocak,[b] Nebih Lolak,[b] Fevzi Topal,[c, d] Ümit Muhammet Koçyiğit,[e] Cüneyt Türkeş,[f] Mesut Işık,*[g] and Şükrü Beydemir[h, i]

The present study focused on the synthesis and characterization of novel pyrazole carboxamide derivatives (**SA1-12**). The inhibitory effect of the compounds on cholinesterases (ChEs; AChE and BChE) and carbonic anhydrases (*h*CAs; *h*CA I and *h*CA II) isoenzymes were screened as *in vitro*. These series compounds have been identified as potential inhibitors with a K_I values in the range of 10.69 ± 1.27–70.87 ± 8.11 nM for hCA I, 20.01 ± 3.48–56.63 ± 6.41 nM for hCA II, 6.60 ± 0.62-14.15 ± 1.09 nM for acetylcholinesterase (AChE) and 54.87 ± 7.76–137.20 ± 9.61 nM for butyrylcholinesterase (BChE). These compounds have a more effective inhibition effect when compared to the reference compounds. In addition, the potential binding positions of the compounds with high affinity for ChE and hCAs were demonstrated by *in silico* methods. The results of *in silico* and *in vitro* studies support each other. As a result of the present study, the compounds with high inhibitory activity for metabolic enzymes, such as ChE and hCA were designed. The compounds may be potential alternative agents used as selective ChE and hCA inhibitors in the treatment of Alzheimer's disease and glaucoma.

1. Introduction

Carbonic anhydrase (CA, EC 4.2.1.1) is an essential enzyme involved in cellular metabolism, and it contains zinc as a cofactor. It exists in various organisms, with at least 16 isozymes identified in tissues and cell fluids, particularly in mammals. CA II and CA IX are the most active isozymes in catalyzing carbon dioxide hydration, with CA II predominantly present in red blood cells and organs such as the lung, kidney and eye.[1–3] The reversible reaction between carbon dioxide and bicarbonate, catalyzed by CA, plays a crucial role in pH regulation across different tissues, organs, and organisms.[4–6] It has been scientifically established that CA, which is widely present in organisms, is composed of eight genetically diverse families.[7–9] Among the mammalian isozymes, *h*CA I is prominent in humans and and holds a physiological importance in various processes including electrolyte secretion, pH regulation, tumor formation, and biosynthetic processes.[10–12] *h*CA II, commonly found in the eyes, significantly contributes to aqueous humor secretion by impacting carbon dioxide hydration and ion balance. Glaucoma, characterized by increased intraocular pressure (IOP) leading to irreversible visual impairment, is influenced by risk factors such as race, severe myopia, ocular hypertension, age, and family history.[13–15]

Metabolic enzymes can undergo changes in activity due to diseases, medication use, and metabolic disorders. Pharmacologically induced alterations in the catalytic activity of *h*CA enzymes can occur through the administration of antiglaucoma agents, antiepileptics, diuretics, antiobesity drugs, medications for high altitude sickness, and anticancer/antimetastatic drugs targeting hypoxic tumors.[16–18] The pharmacological effects of these drugs are attributed to the involvement of different *h*CA isoforms in various physiological processes. Despite their structural and functional similarities, these isoforms play distinct roles and are targeted by specific drugs.[19–21] Certain sulfonamides, both systemic and topical, have been utilized as antiglaucoma agents in the treatment of glaucoma for a

[a] *M. Durgun*
Department of Chemistry, Faculty of Arts and Sciences, Harran University, 63290 Şanlıurfa, Turkey
+90 414 318 3000
E-mail: mustafadurgun@harran.edu.tr

[b] *S. Akocak, N. Lolak*
Department of Pharmaceutical Chemistry, Faculty of Pharmacy, Adıyaman University, 02040 Adıyaman, Turkey

[c] *F. Topal*
Department of Food Engineering, Faculty of Engineering and Natural Sciences, Gümüşhane University, 29100 Gümüşhane, Turkey

[d] *F. Topal*
Department of Chemical and Chemical Processing Technologies, Gümüşhane Vocational School, Gümüşhane University, 29100 Gümüşhane, Turkey

[e] *Ü. M. Koçyiğit*
Department of Biochemistry, Faculty of Pharmacy, Sivas Cumhuriyet University, 58140 Sivas, Turkey

[f] *C. Türkeş*
Department of Biochemistry, Faculty of Pharmacy, Erzincan Binali Yıldırım University, 24002 Erzincan, Turkey

[g] *M. Işık*
Department of Bioengineering, Faculty of Engineering, Bilecik Şeyh Edebali University, 11230 Bilecik, Turkey
+90 228 214 2119
E-mail: mesut.isik@bilecik.edu.tr

[h] *Ş. Beydemir*
Department of Biochemistry, Faculty of Pharmacy, Anadolu University, 26470 Eskişehir, Turkey

[i] *Ş. Beydemir*
Bilecik Şeyh Edebali University, 11230 Bilecik, Turkey

Supporting information for this article is available on the WWW under https://doi.org/10.1002/cbdv.202301824

considerable period. These agents act as carbonic anhydrase inhibitors, effectively regulating intraocular pressure (IOP). A systemic compound known as acetazolamide (AAZ) has been proposed as a means to decrease IOP by reducing the secretion of aqueous humor. However, since oral medications may inhibit other *h*CA isoenzymes in the body, they have been associated with diverse side effects. Hence, it is crucial to design and develop novel agents that exhibit varying levels of affinity for each *h*CA isoenzyme to mitigate these adverse effects.

Acetylcholine (ACh) was discovered due to its role as a neurotransmitter in both the central and peripheral cholinergic synapses, where it releases a substance that inhibits the chronotropic effect of inhibitory nerves on the heart. ACh is the first known neurotransmitter and is involved in various functions in the peripheral and central nervous systems, including attention, motivation, arousal, memory, learning, and muscle contraction. It is well known that individuals with Alzheimer's disease (AD) have low levels of ACh in their brains.[22–27] The enzymes responsible for the hydrolysis of ACh are cholinesterases (ChEs), namely acetylcholinesterase (EC 3.1.1.7; AChE), and butyrylcholinesterase (EC 3.1.1.8; BChE). Among these enzymes, AChE is more specific for the neurotransmitter ACh compared to BChE.[28–30] AChE exhibits greater specificity towards the neurotransmitter ACh compared to BChE.[31–33] These enzymes, found in various tissues, neurons, and across many species, including humans, swiftly hydrolyze ACh, a quaternary amine, into choline (Ch) and acetic acid within milliseconds.[34–36] Notably, BChE plays a significant physiological role in hydrolyzing higher choline esters like butyrylcholine. Cholinesterase inhibitors (ChEIs) are crucial in maintaining adequate ACh levels by reducing the catalytic activity of AChE and BChE, which are responsible for ACh breakdown.[37–39] ChEIs are extensively used for treating dementia, particularly in AD patients, as they decrease ACh hydrolysis. Currently, there are several widely employed ChEIs for therapeutic purposes, including donepezil, galantamine, neostigmine, physostigmine, rivastigmine, and tacrine.[40–42] However, these medications carry potential serious side effects, such as vasodilation, bradycardia, weight loss, bronchoconstriction, and miosis.[43]

Pyrazoles as a five-membered heterocycle containing two adjacent nitrogen atoms play a crucial role in the biological activity of many small molecule drugs. They have the ability to modify polarity, hydrogen bond, and modulate lipophilicity at specific sites in the host or pathogen, leading to the inhibition of biological processes associated with disease progression. As a result, pyrazole heterocycles have become essential building blocks in drug design and materials science research.[44–47] In many studies, pyrazole derivatives have been reported as potential treatments for neurodegenerative disorders such as Alzheimer's and Parkinson's disease. Pyrazole-based hybrid structures also have anticancer, cytotoxicity and selective carbonic anhydrase inhibitory activities. Therefore, the design and synthesis of compounds containing pyrazole rings have attracted the attention of researchers.[48,49] In addition, the presence of this fundamental construction unit in different structures leads to diversified applications in several fields, such as technology, agriculture, and dyes industry. Furthermore, the pharmacological potential of the pyrazole moiety has been demonstrated by its presence in pharmacological agents of various therapeutic categories. The anti-inflammatory Celecoxib and Mepirazole, the anti-obesity drug Rimonabant, the antipsychotic CDPPB, Lonazolac, Difenamizole, Betazole, and Fezolamine are some examples of drugs that contain this moiety and exhibit diverse therapeutic activities, including anti-inflammatory, analgesic, and antidepressant effects, amongst others (Figure 1).[50–57] Of the other hand, this heterocyclic ring have gained significant interest as antimicrobial and anticancer agents in recent years since the discovery of natural pyrazole C-glycosides such as Pyrazofurin (Figure 1).[58,59]

In the light of this information, it is clear that the use of carbonic anhydrase isoenzymes and cholinesterase enzyme inhibitors is a common approach in the treatment of glaucoma and AD. Therefore, the design, development and synthesis of new compounds with alternative inhibitory potential against carbonic anhydrase isoenzymes, AChE and BChE have attracted the attention of researchers. It is important that compounds exhibiting high inhibitory potential have appropriate chemical structures and bioactive properties in order to interact effectively with the active site of these enzymes. Therefore, designing compounds with optimal properties that facilitate targeted enzyme inhibition has become a focus. There are limited studies in the literature on the screening of inhibitory potentials of pyrazole carboxamide derivatives on ChEs and carbonic anhydrase isoenzymes. In the study, the novel pyrazole carboxamide derivatives (**SA1-12**) were designed, synthesized and were thoroughly characterized using various spectroscopic and analytic methods, including FT-IR, ^{1}H-NMR, ^{13}C-NMR, and melting point analysis. The inhibitory effect of synthesized compounds against ChEs and *h*CA isoenzymes was assessed as *in vitro* and *in silico* studies.

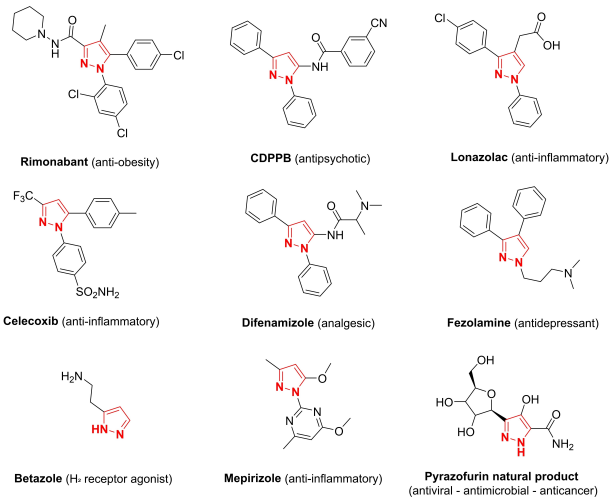

Figure 1. Natural and synthetic drugs and clinical candidates containing the pyrazole moiety.

2. Results and Discussion

2.1. Chemistry

Numerous studies have shown that pyrazole scaffolds possess potent inhibitory activities against cholinesterase and carbonic anhydrase hCA I, hCA II enzymes.[60,61] Moreover, İn our previous studies ureido-substituted derivatives with sulfamethazine backbone showed good inhibitory activity against acetylcholinesterase (AChE) and butyrylcholinesterase (BChE).[62] Additionally, in another study we conducted, it was found that bis-ureido-substituted sulfaguanidines exhibited potent inhibition on hCA I, hCA II and significant inhibitory activity on the acetylcholinesterase (AChE) enzyme.[63] Based on this information, in this work we synthesized novel pyrazole derivatives linked to sulfamethazine (**SM**) or sulfaguanidine (**SG**) in order to investigate their inhibitory activities against ChEs and hCA isoenzymes. For this purpose, a series of novel pyrazole carboxamide derivatives were prepared in this study by the reaction of diazotization with appropriate sulfonamide derivatives **a (1–2)** followed by the reaction with malononitrile in a sodium acetate in water at 0–5 °C. Next, the obtained intermediate **c (1–2)** was treated with substituted semicarbazides **d (1–6)** (that were prepared according to the procedure described by Hron and Jursic)[64] in EtOH at 60 °C temperature for 6 hours giving the desired pyrazole carboxamide derivatives **(SA1-12)** with 62–85% yield. (Scheme 1).

The resulting sulfamethazine (**SM**) or sulfaguanidine (**SG**) derivatives, pyrazole carboxamide derivatives (**SA1-12**), were characterized using FT-IR, ^{1}H-NMR, ^{13}C-NMR, and melting point analysis. Compounds **SA1-12** were observed to be a single spot in the ethyl acetate/petroleum ether (7/3) solvent system in thin layer chromatography and to have a single melting point, and no other impurities other than the product were found in the spectra.

The structural evidence obtained by infrared spectroscopy of synthesized pyrazole carboxamide derivatives is fully consistent with their assignments. Notably, the significant bands appear within the ranges of 1128–1347 (S=O), 1693–1719 (C=O), and 3232–3480 (–NH–) cm^{-1}. The ^{1}H-NMR spectrum of compounds **SA1-6** (sulfamethazine (**SM**) derivatives), gave singlet proton at δ 2.23–2.24 ppm corresponding to methyl protons of sulfamethazine. Also, compounds **SA-3** and **SA-4** showed a singlet peak at δ 2.26 and 2.28 ppm, respectively. Two broad spectrums were observed with the compounds at δ 6.02-6.12 and 6.37–6.48 ppm, corresponding to the $–NH_2$ groups on the pyrazole ring. These peaks confirm the cyclization product of our synthesized compounds. The aromatic spectrums were observed around δ 6.72–8.03 ppm. Another specific peak of –NH– was observed as singlet peak around δ 9.42–9.99 ppm. Also, ^{13}C-NMR of compounds **SA1-6** (sulfamethazine (**SM**) derivatives) displayed the methyl carbon at δ 22.97–23.37 ppm and carbonyl carbons at δ 167.71–167.82 ppm, confirming the structure. On the other hand, compounds **SA7-12** (sulfaguanidine (**SG**) derivatives) exhibited a broad spectrum at δ 6.20–6.25 ppm, corresponding to the $–NH_2$ spectrum of the pyrazole ring. Another broad spectrum was also observed at δ 6.73–6.74 ppm, indicating the presence of the guanidine group. Furthermore, the singlet for –NH– was observed at δ 9.47–9.99 ppm.

2.2. Biological Evaluation

Pyrazoles play a vital role in the composition of various heterocyclic compounds, offering a broad range of biological

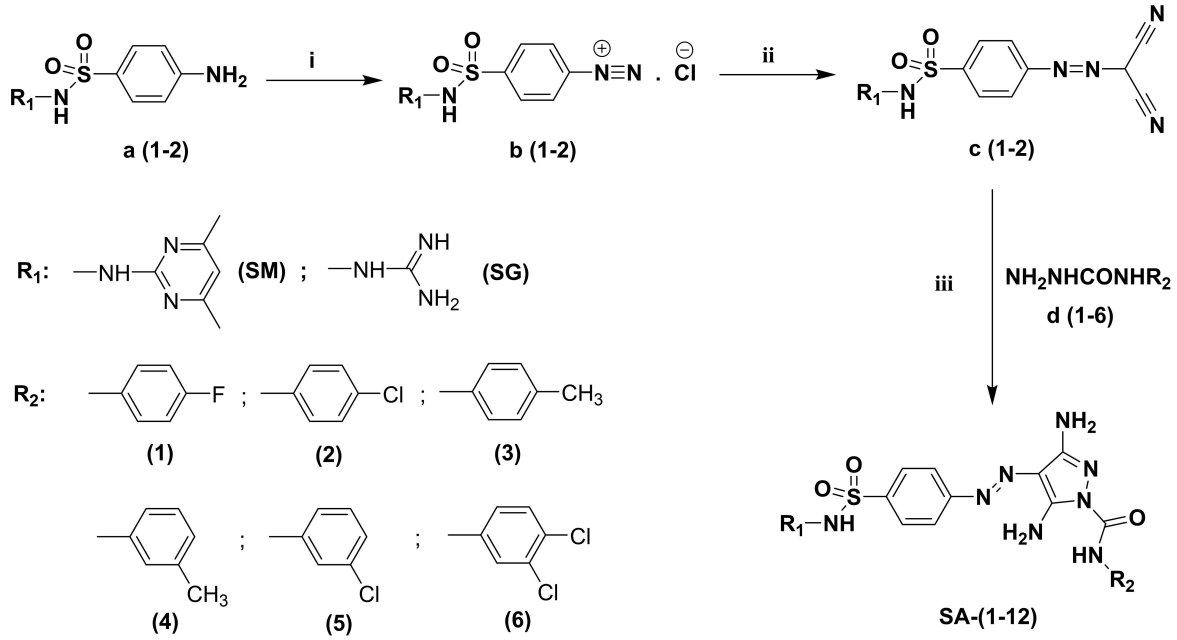

Scheme 1. General synthetic route for the synthesis of pyrazole carboxamide derivatives. Reagents and conditions:(i) HNO_2 / HCl, H_2O, 0 to 5°C; (ii) Malononitrile, MeOH, sodium acetate, 0 to 10°C; (iii) EtOH, reflux, 6h.

activities and medicinal properties. The pyrazole compounds exhibit specific properties including antiviral, antitumor, antidepressant, anti-inflammatory, and antioxidant activities. In the medical sector, pyrazoles are utilized as key components in drugs such as Celebrex, Zerbaxa and Viagra.[65–67] Therefore, it is important to design alternative pyrazole derivatives with different selectivity towards ChEs and *h*CA isoenzymes.

A series of novel pyrazole carboxamide derivatives containing sulfonamide scaffold were synthesized and their inhibition activity against ChEs and hCA isoenzymes was evaluated. The structure of the new pyrazole carboxamide derivatives synthesized as a ChEs and *h*CA isoenzymes inhibitor is presented in Figure 2.

Numerous studies in the literature focus on the synthesis of pyrazole derivatives and their inhibitory effects on ChEs and *h*CAs. In a recent study, novel pyrazole derivatives were synthesized, and it was demonstrated that these compounds exhibit effective inhibition against AChE enzymes as well as cytosolic *h*CA I and II. The pyrazole derivatives showed an inhibitory effect with K_I values in the range of 48.94 ± 9.63–116.05 ± 14.95μM for AChE, 1.03 ± 0.23–22.65 ± 5.36 μM for *h*CA I and 1.82 ± 0.30–27.94 ± 4.74 μM for *h*CA II.[68] In a study, some new some pyrazole derivatives were synthesized. The synthesized compound groups showed effective inhibition profiles with K_I values of 5.13–67.39 nM against *h*CA I and *h*CA II.[69] A series of pyrazole-based carbohydrazide hybrids were synthesized. The synthesized derivatives showed an inhibitory effect with K_I values in the range 572.8-10000 nM (*h*CA I), 6.8–10000 nM (*h*CA II), and 10.1–10000 nM (*h*CA IX).[48] In other literature studies, the results were expressed as follows: The fluorosulfate-containing pyrazole heterocycles compounds showed strong BuChE and hBChE inhibition with IC_{50} of 0.79 μM and 6.59 μM.[70] Coumarin-pyrazole hybrids have potential AChE inhibitory activities with IC_{50} values of 4.41 ± 0.53 and 5.04 ± 0.96 μg/ml.[71] The δ-sultone-fused pyrazole and tricyclic pyrazole compounds were identified as high selective BChE inhibitors with IC_{50} of 8.3 and 7.7 nM[72] and IC_{50} in the range of 1–6 μM, respectively.[73] In the literature studies mentioned above, the inhibition effect of prazole-containing compounds on ChEs and *h*CA isoenzymes was found to be high. In the present study, the inhibition effect of carboxamide derivatives containing pyrazole rings on the enzymes is compatible with the literature studies and is more effective.

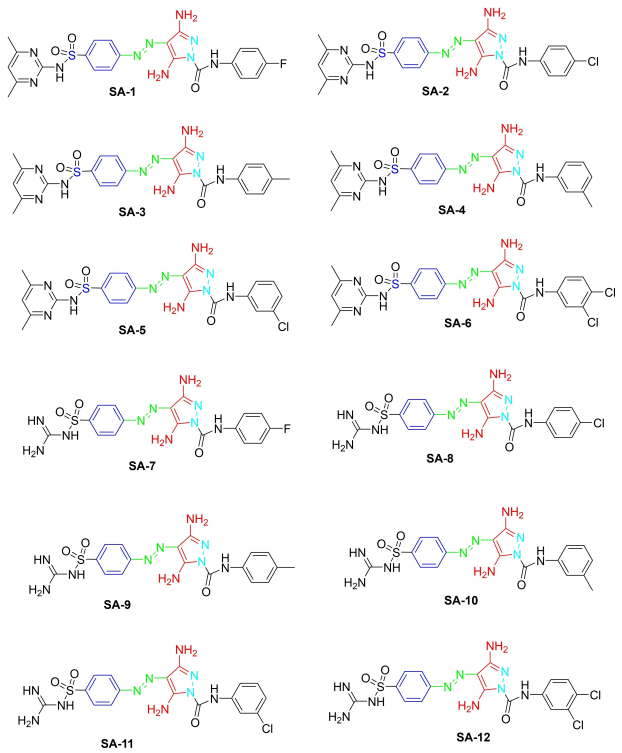

Figure 2. Structure of a novel pyrazole carboxamide derivative synthesized as a ChEs and *h*CA isoenzymes inhibitor.

The sulfonamides are generally non-competitive CA inhibitors. Moreover, examining the initial rate kinetics of CA-catalyzed 4-nitrophenyl acetate hydrolysis displayed that mainly primary sulfonamide inhibitors were non-competitive.[74] Since the sulfonamides in this study are different types than they are secondary, they can also cause competitive and non-competitive inhibition. Enzyme kinetic analyses were conducted on pyrazole carboxamide derivatives against ChEs and *h*CA isoenzymes to ascertain inhibition type and K_I values. Inhibition types encompass reversible and irreversible categories, with subtypes like uncompetitive, competitive, non-competitive, and mixed inhibition. These inhibition subtypes are discerned through Lineweaver-Burk plots.[3-6] This enzyme kinetics study indicates that derivatives act as reversible, competitive and non-competitive inhibitors of hCA I and hCA II enzymes. Compounds **SA1-3** and **SA8** showed competitive inhibition effect for hCA I enzyme, while all other compounds showed non-competitive inhibition effect. Moreover, compound **SA1** caused competitive inhibition for the hCA II enzyme while the others (**SA2-12**) exhibited non-competitive inhibition. Compound **SA12** functions as a non-competitive inhibitor for the BChE enzyme, while all other compounds (**SA1-SA11**) are non-competitive inhibitors for this enzyme and all compounds (**SA1-SA12**) are non-competitive inhibitors for the AChE enzyme. In this context, we present the inhibitory effects of pyrazole carboxamide derivatives (**SA1-12**) on the activity of ChEs and *h*CA isoenzymes *in vitro*. The corresponding results are summarized in Table 1. Besides, IC50 plots and K_I curves of the compounds (**SA1-12**) are presented as supporting information (Supplementary Material Figures S1–24).

The present study synthesized a series of novel pyrazole carboxamide derivatives, and their inhibitory effects on metabolic enzymes were investigated. The derivatives demonstrated significant inhibitory activity against both ChEs and *h*CAs, acting at the nanomolar (nM) level. The K_I values for *h*CA I ranged from 10.69 ± 1.27–70.87 ± 8.11 nM, while for *h*CA II, they ranged from 20.01 ± 3.48–56.63 ± 6.41 nM. Notably, the newly synthesized derivatives exhibited more effective inhibition than the reference compound AAZ (K_Is of 412.13 ± 8.96 nM and 98.28 ± 1.69 nM for *h*CA I and II, respectively) *h*CAs. Among the synthesized compounds, **SA9** displayed the highest inhibitory potential against *h*CA I with a K_I value of 10.69 ± 1.27 nM which is approximately 38 times more potent than the AAZ. On the

Table 1. Inhibition data of important metabolic enzymes with the novel pyrazole carboxamide derivatives (**SA1-12**) and reference compounds THA and AAZ.

Compound ID	AChE [a]		BChE [a]		*h*CA I [a]		*h*CA II [a]	
	IC_{50} (nM)	K_I (nM)	IC_{50} (nM)	K_I (nM)	IC_{50} (nM)	K_I (nM)	IC_{50} (nM)	K_I (nM)
SA1	27.86 ± 0.53	7.36 ± 0.79	77.38 ± 4.47	79.58 ± 13.73	52.19 ± 8.19	53.78 ± 8.15	61.06 ± 6.85	48.54 ± 9.24
SA2	32.82 ± 0.99	7.34 ± 0.63	140.40 ± 2.65	72.31 ± 11.84	25.61 ± 2.50	19.76 ± 3.30	43.51 ± 1.29	56.63 ± 6.41
SA3	38.11 ± 1.41	12.01 ± 1.37	111.20 ± 4.59	79.10 ± 8.88	16.26 ± 0.48	14.84 ± 2.44	32.02 ± 2.54	42.88 ± 5.32
SA4	36.19 ± 0.29	8.98 ± 0.49	132.80 ± 1.53	54.87 ± 7.76	22.80 ± 1.13	26.05 ± 3.04	42.58 ± 3.03	51.86 ± 7.46
SA5	34.00 ± 1.27	7.56 ± 0.75	113.20 ± 2.59	73.79 ± 8.31	35.11 ± 1.53	36.26 ± 4.73	32.70 ± 1.90	31.74 ± 5.62
SA6	32.67 ± 1.01	6.60 ± 0.62	127.70 ± 3.52	68.94 ± 7.02	33.27 ± 1.57	30.87 ± 5.52	33.56 ± 1.30	31.40 ± 4.95
SA7	41.48 ± 1.25	8.19 ± 0.54	158.20 ± 2.84	93.61 ± 7.31	47.74 ± 0.97	70.87 ± 8.11	32.33 ± 1.73	47.70 ± 6.92
SA8	42.12 ± 1.60	6.78 ± 0.46	165.00 ± 5.19	65.12 ± 7.29	23.09 ± 2.15	26.90 ± 3.50	26.45 ± 1.03	30.48 ± 4.52
SA9	41.40 ± 0.83	14.15 ± 1.09	162.10 ± 2.88	74.37 ± 8.94	10.95 ± 0.01	10.69 ± 1.27	22.45 ± 0.06	20.01 ± 3.48
SA10	40.26 ± 1.10	10.41 ± 0.81	155.00 ± 2.47	92.14 ± 10.40	18.54 ± 0.22	14.59 ± 2.71	21.58 ± 0.55	20.06 ± 3.23
SA11	37.93 ± 0.49	10.40 ± 1.08	145.50 ± 3.53	86.34 ± 9.43	20.17 ± 0.73	18.07 ± 2.89	28.88 ± 0.86	32.89 ± 5.46
SA12	38.20 ± 1.32	7.69 ± 0.73	145.00 ± 2.03	137.20 ± 9.61	23.89 ± 1.49	25.86 ± 4.30	35.54 ± 1.13	45.97 ± 6.97
THA[b]	162.31 ± 3.62	112.03 ± 12.42	208.03 ± 13.36	172.03 ± 32.42	–	–	–	–
AAZ [c]	–	–	–	–	246.60 ± 2.00	412.13 ± 8.96	102.30 ± 0.39	98.28 ± 1.69

[a] The test results were expressed as means of triplicate assays ± SEM. [b] Tacrine. [c] Acetazolamide.

other hand, compound **SA7** showed lower potency with a K_I value of 70.87 ± 8.11 nM. For *h*CA II, compound **SA9** exhibited high inhibitory potential with a K_I value of 20.01 ± 3.48 nM which is approximately 38 times more potent than the AAZ. On the other hand, compound **SA2** showed lower potency with a K_I value of 56.63 ± 6.41 nM (Table 1). The K_I values for AChE ranged from 6.60 ± 0.62–14.15 ± 1.09 nM, while for BChE, they ranged from 54.87 ± 7.76–137.20 ± 9.61 nM. Notably, the synthesized derivatives exhibited more effective inhibition than the reference compound THA (K_Is of 112.03 ± 12.42 nM and 172.03 ± 32.42 nM for AChE and BChE, respectively) against ChEs. Among the synthesized compounds, compound **SA6** displayed the highest inhibitory potential against AChE with a K_I value of 6.60 ± 0.62 nM which is approximately 17 times more potent than the THA. On the other hand, compound **SA9** showed inhibitory potency with a K_I value of 14.15 ± 1.09 nM which is approximately 8 times more potent than the THA. For BChE, compound **SA4** exhibited high inhibitory potential with a K_I value of 54.87 ± 7.76 nM which is approximately 3.1 times more potent than the THA. On the other hand, compound **SA12** showed lower potency with a K_I value of 137.20 ± 9.61 nM (Table 1). Upon evaluating the results, all compounds showed an inhibitory effect against both ChE's and *h*CAs. It is understood that one of the prominent among these compounds, non-competitive inhibitor **SA9** *h*CA I and II isoenzymes, is more selective against *h*CA I'. At the same time, this compound has a high inhibitory effect on ChEs and is more selective to AChE than BChE.

The inhibition data obtained from the results of this study show that the synthesized derivatives are more effective than the reference compounds. In addition, these derivatives exhibit similar or higher inhibitory effects than many compounds reported in the literature. These significant effects in inhibitory activity increase the potential of new pyrazole derivatives to be promising candidates for further research in enzyme inhibition. In addition, these data are essential regarding of the importance of structural modifications of new compounds that can be used in treating glaucoma and AD and to guide future research and alternative drug development studies in these areas.

The structure-activity relationship (SAR) study showed against ChEs and *h*CAs potent inhibitory activity of compounds containing the pyrazole carboxamide derivatives sulfamethazine (SM; **SA1-6**) group and sulfaguanidine (SG; **SA7-12**) group. We can say that the change may result from the R_2 variable substitution pattern on the pyrazole carboxamide. Among these compounds, compound **SA6** (K_i: 6.60 ± 0.62 nM) exhibited the most potent inhibition of AChE with the presence of the 3,4-diCl group. At the same time, the **SA12** compound with a 3,4-diCl group was found to be effective among the SG group compounds with a Ki value of 7.69 ± 0.73. In contrast, compound **SA4** displayed the most potent inhibition of BChE with the presence of the 3-Me group. When the activities of the compounds on *h*CA I and II isoforms are examined, it is seen that the presence of methyl groups at positions 3 and 4 increases the activity. Compound **SA9** showed the most potent inhibition of both *h*CA I (K_i: 10.69 ± 1.27 nM) and *h*CA II ((K_i: 20.01 ± 3.48nM) isoforms with the presence of the 4-Me group. If you pay attention, it can be said that the compounds that show the most potent inhibitory properties against ChEs are in the SM group, while against *h*CAs, they are in the SG group. Since Sulfonamides in general show inhibitory effects as a class of compounds studied for their inhibitory effects on hCA, the results obtained show that these compounds are more selective

towards the hCA enzyme compared to AChE and BChE. Another exciting aspect is that although the compounds tested here do not contain a free sulfonamide group (-SO_2NH_2)[75] that binds directly to the Zn^{2+} metal center of *h*CAs, compounds **SA3** (for *h*CA I) and **SA1** (for *h*CA II) were still able to inhibit these enzymes, as seen in molecular docking studies. *In silico* molecular docking simulations have shown that in addition to hydrogen bonding and specific favorable hydrophobic interactions, these target compounds can inhibit the enzyme by fitting into the entrance of the active site such that the aryl group is displaced.

2.3. Molecular Docking Studies

The binding of the synthesized compounds should occur at the active site.[76] Therefore, a molecular docking study of the most active compounds showing competitive inhibition on the enzymes was performed. Therefore, we conducted in silico docking studies utilizing the Small-Molecule Drug Discovery Suite 2023–2 for **SA6**, **SA4**, **SA3**, and **SA1** as representatives of molecules in the series to understand these inhibitors' expected binding interactions with AChE, BChE, *h*CA I, and *h*CA II enzymes, respectively. Fortunately, a multitude of X-ray crystal structures of ChEs and *h*CAs and are at our disposal, and we meticulously assessed their binding site interactions to determine suitable structures for employment in docking simulations. Subsequently, we opted for the 3D structures of ChEs and *h*CAs and that were bound with the reference drugs tacrine (THA, PDB IDs of 7XN1[77] and 4BDS[78] for AChE and BChE, respectively) and AAZ (AZM, PDB IDs of 1AZM[79] and 3HS4[80] for *h*CA I and *h*CA II, respectively) for further examination based on the chemical scaffolds of the cocrystallized ligands and the conformations of the binding site residues. The effectiveness of the docking setup was validated by re-docking the co-crystallized native ligands THA and AZM into the enzyme binding sites. The reliability of the docking methodology was demonstrated by minimal RMSD values (0.26, 0.12, 0.22, and 0.99 Å for 7XN1, 4BDS, 1AZM, and 3HS4, respectively), as well as the ability of the docking poses of the co-crystalized ligands to replicate all essential interactions.

Here, **SA6**, **SA4**, **SA3**, and **SA1** have established primary contacts through H-bonding and pi-pi stacking interactions. These inhibitors have docking scores of −9.686, −5.306, −2.958, and −6.376 kcal/mol with 7XN1, 4BDS, 1AZM, and 3HS4, respectively. Herein, the potent inhibitor **SA6** versus AChE has made H-bonds with Trp86 (water-mediated 2.46 Å) and Ser125 (water-mediated 1.93 Å), Tyr337 (2.14 Å), Tyr341 (3.41 Å), and a water molecule at a distance of 2.43 Å. In addition, it has formed pi-pi stacking interactions with Tyr72, Trp86, Tyr337, and Tyr341 (Figure 3). The most active compound against BChE, **SA4**, has formed H-bonds with Gly116 (water-mediated 2.43 Å), Ala328 (2.03 Å), and a water molecule at a distance of 2.43 Å. Furthermore, it has formed a pi-pi stacking interaction with Trp82 residue, as shown in Figure 4. Compound **SA3** and *h*CA I have exhibited pi-pi stacking interaction with Phe91 residue (Figure 5). Compound **SA1** has

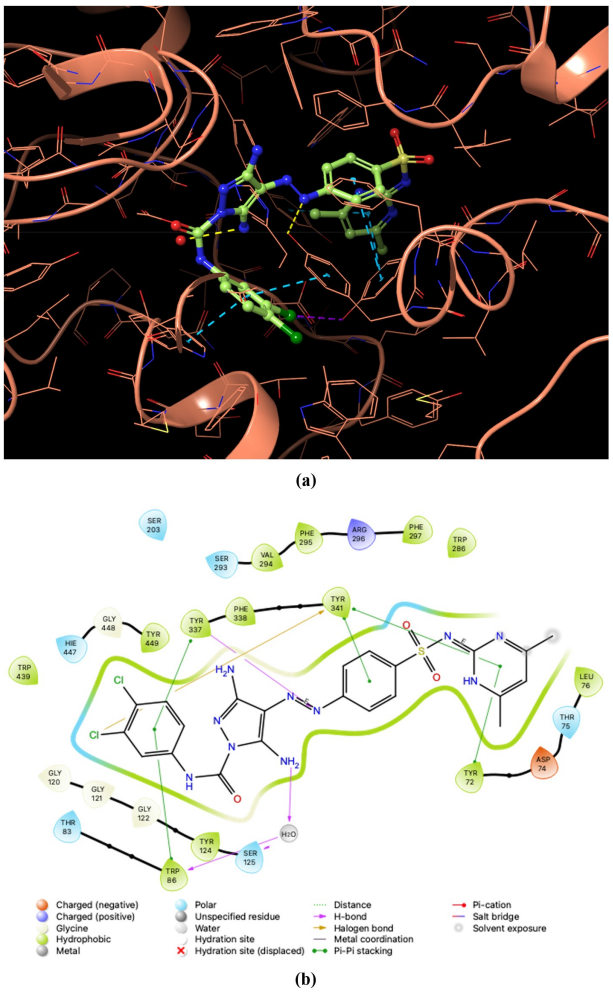

Figure 3. (a) 3D and **(b)** 2D binding interaction patterns of compound **SA6** (3,5-diamino-*N*-(3,4-dichlorophenyl)-4-((4-(*N*-(4,6-dimethylpyrimidin-2-yl)sulfamoyl)phenyl)diazenyl)-1*H*-pyrazole-1-carboxamide) with active site residues of acetylcholinesterase enzyme (RCSB PDB code 7XN1).

made an H-bond with Thr200 (1.97 Å) residue and a water molecule (2.17 Å) in the center of *h*CA II's active site, while Phe131 residue interacted through pi-pi stacking, as depicted in Figure 6. In conclusion, these inhibitors' docking scores and binding poses have proven their potency against ChEs and *h*CAs.

ADME/T-related parameters were determined for novel pyrazole carboxamide derivatives (**SA1-12**), and the results are summarized in Table 2. Additionally, diagrams showing "drug-likeness" descriptors for **SA6**, **SA4**, **SA3**, and **SA1** against AChE, BChE, *h*CA I, and *h*CA II, respectively, are given in Figure 7.

Materials and Methods

General Synthetic Procedure for the Compounds SA1-12

In order to create a diazonium solution of sulfamethazine (SM) and sulfaguanidine (SG), a mixture of 50 mmol of these substances, 15 ml of concentrated hydrochloric acid, and 30 ml of water was cooled to 0–5 °C. Sodium nitrite (60 mmol) in 20 ml of water was

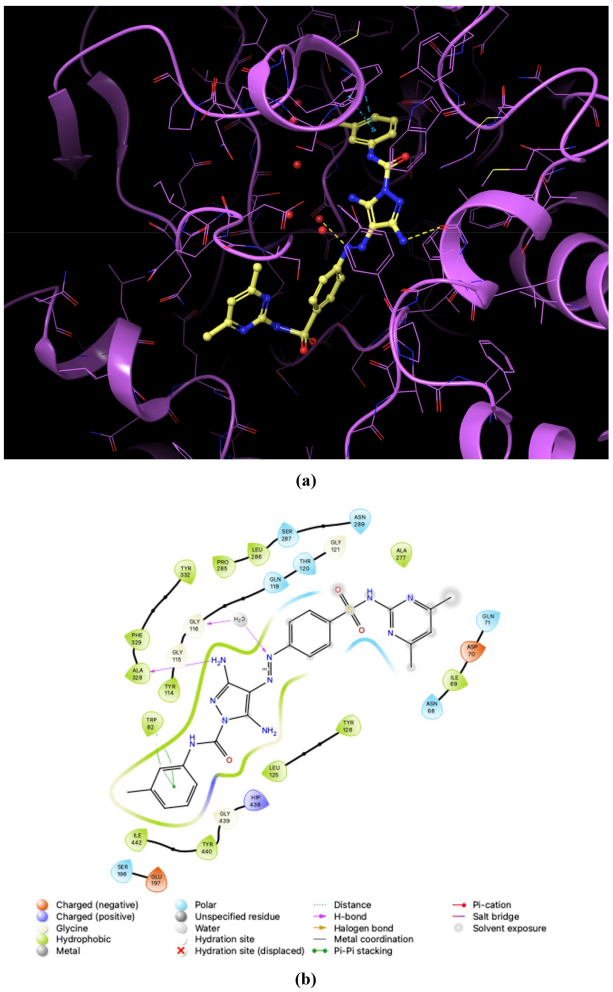

Figure 4. (a) 3D and **(b)** 2D binding interaction patterns of compound **SA4** (3,5-diamino-4-((4-(*N*-(4,6-dimethylpyrimidin-2-yl)sulfamoyl)phenyl)diazenyl)-*N*-(m-tolyl)-1*H*-pyrazole-1-carboxamide) with active site residues of butyrylcholinesterase enzyme (RCSB PDB code 4BDS).

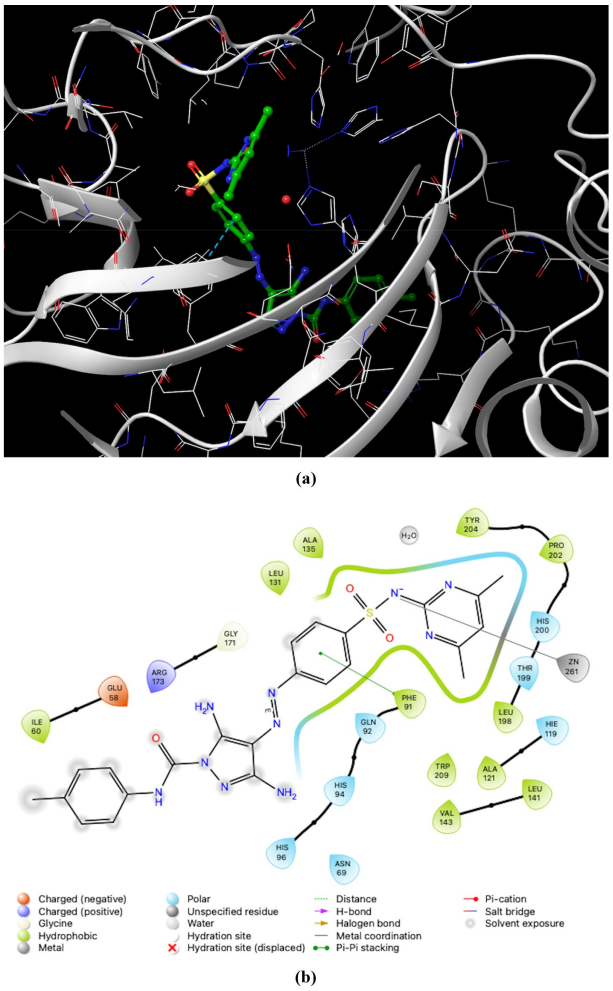

Figure 5. (a) 3D and **(b)** 2D binding interaction patterns of compound **SA3** (3,5-diamino-4-((4-(*N*-(4,6-dimethylpyrimidin-2-yl)sulfamoyl)phenyl)diazenyl)-*N*-(p-tolyl)-1*H*-pyrazole-1-carboxamide) with active site residues of carbonic anhydrase I isoenzyme (RCSB PDB code 1AZM).

then added dropwise to the mixture over a period of 15–20 minutes while it was continuously stirred. After stirring for around 20 minutes at the same low temperature, a diazonium solution was created and added to a separate solution of malononitrile (prepared by dissolving 50 mmol of malononitrile in 15 ml of methanol) by adjusting the pH to 6–7 using saturated sodium acetate. The resulting mixture was stirred at a low temperature (0–5 °C) for 3 hours, then kept overnight at room temperature in the dark. After filtering the mixture and washing it several times with cold water, it was crystallized from ethanol and used for the next step of the reaction without purification. Then, diazo-containing malononitrile derivatives (1 mmol) dissolved in 10 ml of ethanol and substituted semicarbazides (1 mmol) (N-(4-fluorophenyl)hydrazinecarboxamide for SA-1 and SA-7; N-(4-Chlorophenyl)hydrazinecarboxamide for SA-2 and SA-8; N-(p-tolyl)-hydrazinecarboxamide for SA-3 and SA-9; N-(m-tolyl)-hydrazinecarboxamide for SA-4 and SA-10; N-(3-Chlorophenyl)-hydrazinecarboxamide for SA-5 and SA-11; N-(3,4-dichlorophenyl)hydrazinecarboxamide for SA-6 and SA-12) were added and the mixture was refluxed for around 6 hours with TLC monitoring. The solution was then filtered off and washed several times with water. Finally, the resulting product was dried under vacuum, stored in a dark location, and fully characterized using FT-IR, ^{1}H-NMR, ^{13}C-NMR, and melting point analysis (Scheme 1). Besides, ^{1}H-NMR and ^{13}C-NMR spectra of compounds (**SA1-12**) are presented as supporting information (Supplementary Material Figures S25–48).

3,5-diamino-4-((4-(N-(4,6-dimethylpyrimidin-2-yl)sulfamoyl)phenyl)diazenyl)-N-(4-fluorophenyl)-1H-pyrazole-1-carboxamide (SA1)

Yield: 65%; Color: orange solid; Melting Point: 237–238 °C; FT-IR (cm^{-1}): 3462, 3436, 3363, 3340 (NH), 1709 (C=O), 1608, 1338, 1150 (symmetric) (S=O), 1078; ^{1}H-NMR (DMSO-d_6, 500 MHz, δ ppm): 9.71 (s, 1H, –NH–), 8.01 (d, J = 9.0 Hz, 2H, Ar–H), 7.89 (d, J = 9.0 Hz, 2H, Ar–H), 7.67–7.64 (m, 2H, Ar–H), 7.18 (t, J = 8.5 Hz, 2H, Ar–H), 6.74 (s, 1H, Ar–H), 6.46 (br.s, 2H, –NH_2), 6.03 (br.s, 2H, –NH_2), 2.24 (s, 6H, –CH_3); ^{13}C-NMR (DMSO-d_6, 125 MHz, δ ppm): 167.71, 160.06, 158.05, 156.55, 155.88, 150.68, 139.10, 133.96, 129.49, 123.08, 120.88, 115.86, 115.68, 115.20, 22.97.

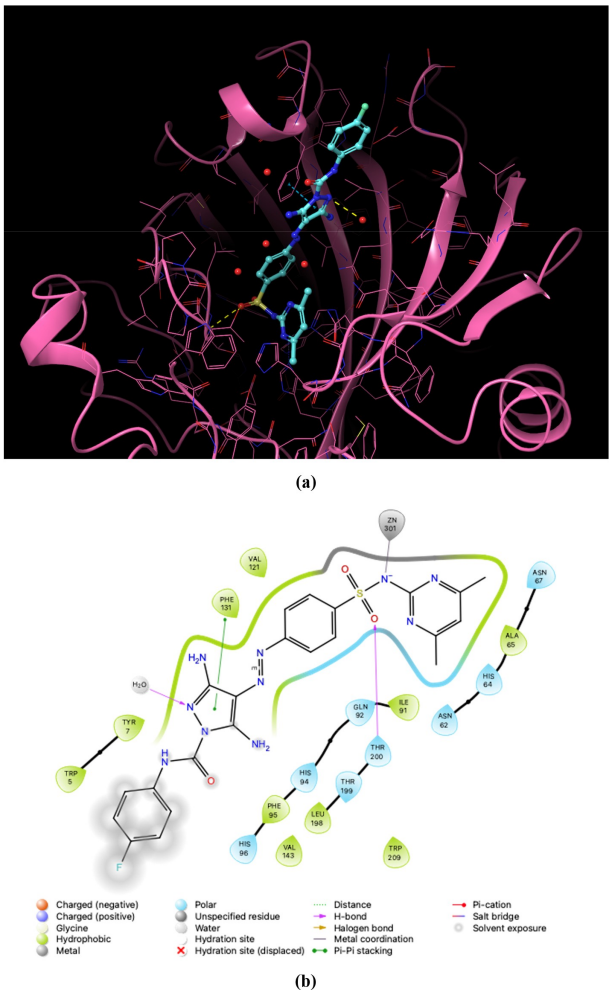

Figure 6. **(a)** 3D and **(b)** 2D binding interaction patterns of compound **SA1** (3,5-diamino-4-((4-(*N*-(4,6-dimethylpyrimidin-2-yl)sulfamoyl)phenyl)diazenyl)-*N*-(4-fluorophenyl)-1*H*-pyrazole-1-carboxamide) with active site residues of carbonic anhydrase II isoenzyme (RCSB PDB code 3HS4).

3,5-diamino-N-(4-Chlorophenyl)-4-((4-(N-(4,6-dimethylpyrimidin-2-yl)sulfamoyl)phenyl)diazenyl)-1H-pyrazole-1-carboxamide (SA2)

Yield: 62%; Color: orange solid; Melting Point: 243–244 °C; FT-IR (cm^{-1}): 3452, 3440, 3354, 3334 (NH), 1713 (C=O), 1618, 1339, 1151 (symmetric) (S=O), 1079; ^{1}H-NMR (DMSO-d_6, 500 MHz, δ ppm): 9.79 (s, 1H, –NH–), 8.01 (d, J = 8.5 Hz, 2H, Ar–H), 7.89 (d, J = 8.5 Hz, 2H, Ar–H), 7.68 (d, J = 8.0 Hz, 2H, Ar–H), 7.39 (d, J = 8.0 Hz, 2H, Ar–H), 6.74 (s, 1H, Ar–H), 6.48 (br.s, 2H, $–NH_2$), 6.02 (br.s, 2H, $–NH_2$), 2.24 (s, 6H, $–CH_3$); ^{13}C-NMR (DMSO-d_6, 125 MHz, δ ppm): 167.74, 156.56, 155.86, 150.49, 148.04, 136.74, 129.49, 128.89, 128.24, 122.55, 120.82, 120.17, 115.66, 115.18, 23.37.

3,5-diamino-4-((4-(N-(4,6-dimethylpyrimidin-2-yl)sulfamoyl)phenyl)diazenyl)-N-(p-tolyl)-1H-pyrazole-1-carboxamide (SA3)

Yield: 77%; Color: orange solid; Melting Point: 249–250 °C; FT-IR (cm^{-1}): 3445, 3363, 3286 (NH), 1711 (C=O), 1617, 1338, 1150 (symmetric) (S=O), 1077; ^{1}H-NMR (DMSO-d_6, 500 MHz, δ ppm): 9.49 (s, 1H, –NH–), 8.01 (d, J = 8.5 Hz, 2H, Ar–H), 7.89 (d, J = 8.5 Hz, 2H, Ar–H), 7.50 (d, J = 8.5 Hz, 2H, Ar–H), 7.14 (d, J = 8.0 Hz, 2H, Ar–H), 6.74 (s, 1H, Ar–H), 6.41 (br.s, 2H, $–NH_2$), 6.05 (br.s, 2H, $–NH_2$), 2.26 (s, 3H, $–CH_3$), 2.24 (s, 6H, $–CH_3$); ^{13}C-NMR (DMSO-d_6, 125 MHz, δ ppm): 167.80, 156.59, 155.90, 150.47, 139.17, 135.06, 133.60, 129.68, 129.63, 129.49, 120.86, 115.09, 114.57, 113.75, 22.98, 20.94.

3,5-diamino-4-((4-(N-(4,6-dimethylpyrimidin-2-yl)sulfamoyl)phenyl)diazenyl)-N-(m-tolyl)-1H-pyrazole-1-carboxamide (SA4)

Yield: 71%; Color: yellow solid; Melting Point: 229–231 °C; FT-IR (cm^{-1}): 3476, 3411, 3363, 3293 (NH), 1705 (C=O), 1621, 1345, 1135 (symmetric) (S=O), 1075; ^{1}H-NMR (DMSO-d_6, 500 MHz, δ ppm): 9.47 (s, 1H, –NH–), 8.02 (d, J = 8.5 Hz, 2H, Ar–H), 7.91 (d, J = 8.5 Hz, 2H, Ar–H), 7.48 (s, 1H, Ar–H), 7.41 (d, J = 7.5 Hz, 1H, Ar–H), 7.21 (t, J = 8.0 Hz, 1H, Ar–H), 6.92 (d, J = 7.5 Hz, 1H, Ar–H), 6.72 (s, 1H, Ar–H), 6.43 (br.s, 2H, $–NH_2$), 6.10 (br.s, 2H, $–NH_2$), 2.28 (s, 3H, $–CH_3$), 2.24 (s, 6H, $–CH_3$); ^{13}C-NMR (DMSO-d_6, 125 MHz, δ ppm): 167.72, 156.55, 155.90, 150.42, 139.18, 138.53, 137.52, 129.50, 128.86, 125.20, 121.25, 120.88, 117.87, 115.32, 113.75, 23.37, 21.24.

3,5-diamino-N-(3-Chlorophenyl)-4-((4-(N-(4,6-dimethylpyrimidin-2-yl)sulfamoyl)phenyl)diazenyl)-1H-pyrazole-1-carboxamide (SA5)

Yield: 68%; Color: dark yellow solid; Melting Point: 239–240 °C; FT-IR (cm^{-1}): 3480, 3415, 3370, 3334 (NH), 1703 (C=O), 1622, 1347, 1135 (symmetric) (S=O), 1075; ^{1}H-NMR (DMSO-d_6, 500 MHz, δ ppm): 9.47 (s, 1H, –NH–), 8.02 (d, J = 8.5 Hz, 2H, Ar–H), 7.91 (d, J = 8.5 Hz, 2H, Ar–H), 7.48 (s, 1H, Ar–H), 7.41 (d, J = 7.5 Hz, 1H, Ar–H), 7.21 (t, J = 8.0 Hz, 1H, Ar–H), 6.92 (d, J = 7.5 Hz, 1H, Ar–H), 6.72 (s, 1H, Ar–H), 6.43 (br.s, 2H, $–NH_2$), 6.10 (br.s, 2H, $–NH_2$), 2.28 (s, 3H, $–CH_3$), 2.24 (s, 6H, $–CH_3$); ^{13}C-NMR (DMSO-d_6, 125 MHz, δ ppm): 167.72, 156.55, 155.90, 150.42, 139.18, 138.53, 137.52, 129.50, 128.86, 125.20, 121.25, 120.88, 117.87, 115.32, 113.75, 23.37, 21.24.

3,5-diamino-N-(3,4-dichlorophenyl)-4-((4-(N-(4,6-dimethylpyrimidin-2-yl)sulfamoyl)phenyl)diazenyl)-1H-pyrazole-1-carboxamide (SA6)

Yield: 65%; Color: orange solid; Melting Point: 232–234 °C; FT-IR (cm^{-1}): 3440, 3357, 3323 (NH), 1719 (C=O), 1640, 1344, 1157 (symmetric) (S=O), 1076; ^{1}H-NMR (DMSO-d_6, 500 MHz, δ ppm): 9.99 (s, 1H, –NH–), 8.03-8.00 (m, 3H, Ar–H), 7.90 (d, J = 8.5 Hz, 2H, Ar–H), 7.66 (d, J = 8.5 Hz, 2H, Ar–H), 7.56 (d, J = 8.0 Hz, 1H, Ar–H), 6.73 (s, 1H, Ar–H), 6.40 (br.s, 2H, $–NH_2$), 6.10 (br.s, 2H, $–NH_2$), 2.24 (s, 6H, $–CH_3$); ^{13}C-NMR (DMSO-d_6, 125 MHz, δ ppm): 167.82, 156.55, 155.84, 149.40, 138.12, 131.38, 130.95, 129.49, 126.01, 122.16, 121.01, 120.91, 120.17, 115.33, 114.65, 113.76, 22.99.

3,5-diamino-4-((4-(N-carbamimidoylsulfamoyl)phenyl)diazenyl)-N-(4-fluorophenyl)-1H-pyrazole-1-carboxamide (SA7)

Yield: 75%; Color: orange solid; Melting Point: 240–241 °C; FT-IR (cm^{-1}): 3452, 3419, 3334, 3296 (NH), 1702 (C=O), 1610, 1256, 1128 (symmetric) (S=O), 1091; ^{1}H-NMR (DMSO-d_6, 500 MHz, δ ppm): 9.70 (s, 1H, –NH–), 7.89 (d, J = 8.5 Hz, 2H, Ar–H), 7.80 (d, J = 8.5 Hz, 2H, Ar–H), 7.73-7.68 (m, 2H, Ar–H), 7.23-7.18 (m, 2H, Ar–H), 6.74 (br.s, 4H, guanidine), 6.21 (br.s, 4H, $–NH_2$); ^{13}C-NMR (DMSO-d_6, 125 MHz, δ ppm): 158.55, 154.83, 150.56, 143.25, 133.91, 126.99, 123.06, 121.31, 115.88, 115.67, 114.71.

Table 2. Physicochemical, pharmacokinetic, and drug-likeness properties of novel pyrazole carboxamide derivatives (**SA1-12**) by SwissADME platform.

Compound ID	Physicochemical parameters						Pharmacokinetic parameters		Drug-likeness properties	
	MW (g/mol)	Heavy atoms	Rotatable bonds	H-bond acceptors	H-bond donors	MLogP	GI absorption	BBB permeation	Lipinski rule	Bioavailability
SA1	524.53	37	8	9	4	1.57	Low	No	No; 2 violations: MW > 500, NorO > 10	0.17
SA2	540.99	37	8	8	4	1.67	Low	No	No; 2 violations: MW > 500, NorO > 10	0.17
SA3	520.57	37	8	8	4	2.08	Low	No	No; 2 violations: MW > 500, NorO > 10	0.17
SA4	520.57	37	8	8	4	2.08	Low	No	No; 2 violations: MW > 500, NorO > 10	0.17
SA5	540.99	37	8	8	4	1.67	Low	No	No; 2 violations: MW > 500, NorO > 10	0.17
SA6	575.43	38	8	8	4	2.15	Low	No	No; 2 violations: MW > 500, NorO > 10	0.17
SA7	460.45	17	8	8	6	1.12	Low	No	No; 2 violations: NorO > 10, NHorOH > 5	0.17
SA8	476.90	17	8	7	6	1.24	Low	No	No; 2 violations: NorO > 10, HorOH > 5	0.17
SA9	456.48	17	8	7	6	1.24	Low	No	No; 2 violations: NorO > 10, HorOH > 5	0.17
SA10	456.48	17	8	7	6	1.24	Low	No	No; 2 violations: NorO > 10, HorOH > 5	0.17
SA11	476.90	17	8	7	6	1.24	Low	No	No; 2 violations: NorO > 10, HorOH > 5	0.17
SA12	511.35	17	8	7	6	1.74	Low	No	No; 3 violations: MW > 500, orO > 10, NHorOH > 5	0.17

3,5-diamino-4-((4-(N-carbamimidoylsulfamoyl)phenyl)diazenyl)-N-(4-Chlorophenyl)-1H-pyrazole-1-carboxamide (SA8)

Yield: 83%; Color: orange solid; Melting Point: 251–253 °C; FT-IR (cm^{-1}): 3436, 3390, 3313, 3299 (NH), 1693 (C=O), 1265, 1137 (symmetric) (S=O), 1095; ^{1}H-NMR (DMSO-d_6, 500 MHz, δ ppm): 9.80 (s, 1H, –NH–), 7.89 (d, J = 8.5 Hz, 2H, Ar–H), 7.80 (d, J = 8.0 Hz, 2H, Ar–H), 7.72 (d, J = 8.0 Hz, 2H, Ar–H), 7.42 (d, J = 8.0 Hz, 2H, Ar–H), 6.74 (br.s, 4H, guanidine), 6.25 (br.s, 4H, $–NH_2$); ^{13}C-NMR (DMSO-d_6, 125 MHz, δ ppm): 158.54, 155.22, 150.17, 143.23, 136.91, 129.07, 126.98, 122.55, 121.32, 120.57, 115.60, 114.86.

3,5-diamino-4-((4-(N-carbamimidoylsulfamoyl)phenyl)diazenyl)-N-(p-tolyl)-1H-pyrazole-1-carboxamide (SA9)

Yield: 78%; Color: orange solid; Melting Point: 256–257 °C; FT-IR (cm^{-1}): 3433, 3396, 3320, 3303 (NH), 1697 (C=O), 1622, 1260, 1134

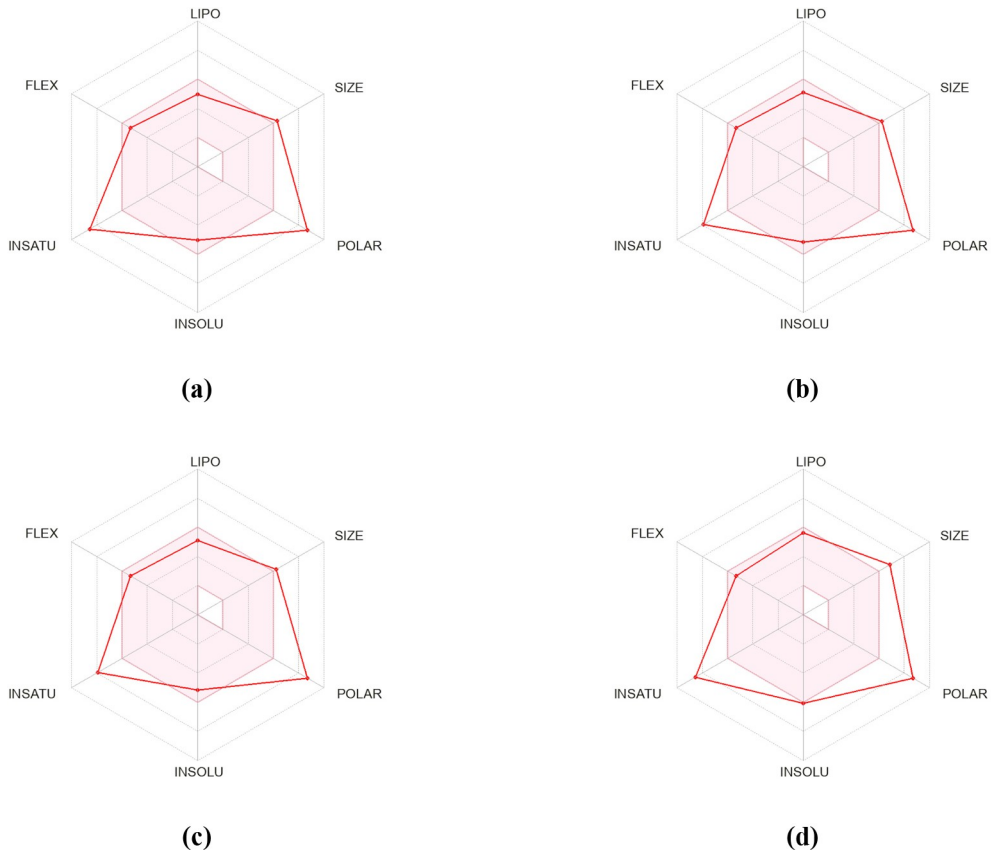

Figure 7. Diagrams showing "drug-likeness" descriptors for compounds **(a) SA1** (3,5-diamino-4-((4-(*N*-(4,6-dimethylpyrimidin-2-yl)sulfamoyl)phenyl)diazenyl)-*N*-(4-fluorophenyl)-1*H*-pyrazole-1-carboxamide), **(b) SA3** (3,5-diamino-4-((4-(*N*-(4,6-dimethylpyrimidin-2-yl)sulfamoyl)phenyl)diazenyl)-*N*-(p-tolyl)-1*H*-pyrazole-1-carboxamide), **(c) SA4** (3,5-diamino-4-((4-(*N*-(4,6-dimethylpyrimidin-2-yl)sulfamoyl)phenyl)diazenyl)-*N*-(m-tolyl)-1*H*-pyrazole-1-carboxamide), and **(d) SA6** (3,5-diamino-*N*-(3,4-dichlorophenyl)-4-((4-(*N*-(4,6-dimethylpyrimidin-2-yl)sulfamoyl)phenyl)diazenyl)-1*H*-pyrazole-1-carboxamide) from novel synthesized pyrazole carboxamide derivatives. The colored zone is a suitable physicochemical space for oral bioavailability. LIPO, lipophilicity; SIZE, molecular weight; POLAR, polarity; INSOLU, insolubility; INSATU, insaturation; FLEX, flexibility.

(symmetric) (S=O), 1092; ^{1}H-NMR (DMSO-d$_6$, 500 MHz, δ ppm): 9.49 (s, 1H, –NH–), 7.86 (d, *J* = 8.5 Hz, 2H, Ar–H), 7.79 (d, *J* = 8.5 Hz, 2H, Ar–H), 7.51 (d, *J* = 8.0 Hz, 2H, Ar–H), 7.15 (d, *J* = 8.0 Hz, 2H, Ar–H), 6.73 (br.s, 4H, guanidine), 6.20 (br.s, 4H, –NH$_2$), 2.26 (s, 3H, –CH$_3$); ^{13}C-NMR (DMSO-d$_6$, 125 MHz, δ ppm): 158.53, 155.07, 150.51, 147.17, 141.86, 135.07, 133.60, 129.64, 127.00, 121.27, 120.85, 120.59, 114.87, 20.94.

3,5-diamino-4-((4-(N-carbamimidoylsulfamoyl)phenyl)diazenyl)-N-(m-tolyl)-1H-pyrazole-1-carboxamide (SA10)

Yield: 69%; Color: orange solid; Melting Point: >300 °C; FT-IR (cm^{-1}): 3462, 3434, 3346, 3320 (NH), 1702 (C=O), 1610, 1252, 1132 (symmetric) (S=O), 1094; ^{1}H-NMR (DMSO-d$_6$, 500 MHz, δ ppm): 9.47 (s, 1H, –NH–), 7.87 (d, *J* = 8.5 Hz, 2H, Ar–H), 7.79 (d, *J* = 8.5 Hz, 2H, Ar–H), 7.49 (s, 1H, Ar–H), 7.41 (d, *J* = 8.0 Hz, 1H, Ar–H), 7.22 (t, *J* = 7.5 Hz, 1H, Ar–H), 6.93 (d, *J* = 7.5 Hz, 1H, Ar–H), 6.74 (br.s, 4H, guanidine), 6.23 (br.s, 4H, –NH$_2$), 2.29 (s, 3H, –CH$_3$); ^{13}C-NMR (DMSO-d$_6$, 125 MHz, δ ppm): 158.49, 155.06, 150.46, 143.19, 138.53, 137.54, 129.10, 127.01, 125.20, 121.24, 120.53, 117.91, 117.21, 114.86, 21.63.

3,5-diamino-4-((4-(N-carbamimidoylsulfamoyl)phenyl)diazenyl)-N-(3-Chlorophenyl)-1H-pyrazole-1-carboxamide (SA11)

Yield: 85%; Color: orange solid; Melting Point: 249–250 °C; FT-IR (cm^{-1}): 3445, 3335, 3323, 3232 (NH), 1713 (C=O), 1623, 1254, 1129 (symmetric) (S=O), 1096; ^{1}H-NMR (DMSO-d$_6$, 500 MHz, δ ppm): 9.85 (s, 1H, –NH–), 7.88 (s, 1H, Ar–H), 7.85 (d, *J* = 6.0 Hz, 2H, Ar–H), 7.79 (d, *J* = 8.5 Hz, 2H, Ar–H), 7.60 (d, *J* = 8.5 Hz, 1H, Ar–H), 7.36 (t, *J* = 8.5 Hz, 1H, Ar–H), 7.16 (d, *J* = 8.0 Hz, 1H, Ar–H), 6.73 (br.s, 4H, guanidine), 6.22 (br.s, 4H, –NH$_2$); ^{13}C-NMR (DMSO-d$_6$, 125 MHz, δ ppm): 158.52, 155.03, 150.56, 143.23, 139.38, 133.48, 130.82, 127.00, 124.11, 121.32, 120.30, 119.36, 115.41, 114.82, 113.41.

3,5-diamino-4-((4-(N-carbamimidoylsulfamoyl)phenyl)diazenyl)-N-(3,4-dichlorophenyl)-1H-pyrazole-1-carboxamide (SA12)

Yield: 68%; Color: orange solid; Melting Point: 234–236 °C; FT-IR (cm^{-1}): 3452, 3429, 3337, 3302 (NH), 1712 (C=O), 1615, 1252, 1132 (symmetric) (S=O), 1092; ^{1}H-NMR (DMSO-d$_6$, 500 MHz, δ ppm): 9.99 (s, 1H, –NH–), 8.04 (s, 1H, Ar–H), 7.87 (d, *J* = 8.5 Hz, 2H, Ar–H), 7.79 (d, *J* = 9.0 Hz, 2H, Ar–H), 7.66 (d, *J* = 6.0 Hz, 1H, Ar–H), 7.57 (d, *J* = 9.0 Hz, 1H, Ar–H), 6.74 (br.s, 4H, guanidine), 6.23 (br.s, 4H, –NH$_2$); ^{13}C-NMR (DMSO-d$_6$, 125 MHz, δ ppm): 158.48, 155.02, 150.55, 143.25, 138.13, 131.39, 130.95, 127.00, 126.00, 122.13, 121.33, 120.99, 120.60, 114.81, 114.49.

Biological Evaluation

AChE/BChE Inhibition Activity

The estimation of the ChEs activities was performed by a modified version of the Ellman's method,[81,82] using acetylthiocholine iodide for AChE and butrylcholine iodide for BChE as the substrates. Acetylcholinesterase from Electrophorus electricus (C2888) and Butyrylcholinesterase from equine serum (C1057) were provided from Sigma-Aldrich Chemie GmbH (Taufkirchen, Germany). The activity data were monitored spectrophotometrically at 412 nm.[83,84]

hCA Isoenzymes Activity

First, purification of *h*CA I and *h*CA II used in this study was performed using a modified procedure based on previous literature.[63] To evaluate the inhibitory effects, the esterase activities of *h*CA isoforms according to Verpoorte's method[85,86] were assessed using the *p*-nitrophenylacetate substrate, which is converted by both isoforms to the *p*-nitrophenolate ion, as previously described in our studies.[87]

In Vitro Inhibition Studies

The inhibition effects of the novel pyrazole carboxamide derivatives (**SA1-12**) were determined with different inhibitor concentrations (at least five) against *h*CA, *h*CA II, AChE and BChE. The IC_{50} of the derivatives was calculated from Activity (%)–[inhibitor] graphs for derivatives. The inhibition types and K_I values were found by Michaelis-Menten graphs[88,89] and Lineweaver and Burk's curves.[90,91]

Molecular Docking Studies

Molecular docking analyses were carried out to investigate the synthesized inhibitors against ChE and *h*CA complexes using the Small-Molecule Drug Discovery Suite 2023–2 for Mac (Schrödinger, LLC, NY, USA). The protein crystal structures, namely PDB IDs 7XN1,[77] 4BDS,[78] 1AZM,[79] and 3HS4[80] for AChE, BChE, *h*CA I, and *h*CA II, respectively, were retrieved from the RCSB protein data bank. These structures were processed using default settings with the Protein Preparation Workflow panel.[92] The resultant protein-ligand complexes were then defined as the binding site. The structures of these pyrazole carboxamide derivatives were sketched using the ChemDraw program V21 for Mac (PerkinElmer, Inc., Waltham, MA, USA). The LigPrep tool in the OPLS force field[93,94] was employed to prepare the three-dimensional structures of the inhibitors as per default options. Furthermore, the appropriate ionization states at pH 7.4 ± 0.5 were determined using Epik.[95,96] The Receptor Grid Generation module[97] was utilized to establish the receptor grids by centering on the co-crystallized ligands within the protein structures.[98,99] The validity of the ChEs and *h*CAs binding site was also confirmed using SiteMap software,[100] which determined the best score for the target ligands, THA and AZM. The initial docking simulation was executed by means of the Glide Ligand Docking panel[101,102] employing the Standard Precision (SP) mode.[103] Following the docking simulation, each docked conformation underwent post-docking minimization. Subsequently, the docked conformations obtained from the previous step were utilized to perform the docking procedure using the Extra Precision (XP) method.[104] Additionally, the ADME/T-related parameters of the all derivatives (**SA1-12**) were determined using the SwissADME platform[105] (Table 2).

Statistical Studies

The data analysis and graph generation were performed using GraphPad Prism version 8 for Mac (GraphPad Software, La Jolla, California, USA). The goodness of fit for enzyme inhibition models was compared using the extra sum-of-squares F test and the AICc approach. The results were presented as the mean ± standard error of the mean, along with 95% confidence intervals. Statistical significance was determined when the *p*-value was less than 0.05.

4. Conclusions

In conclusion, the focus has been on the synthesis and evaluation of novel pyrazole carboxamide derivatives as inhibitors of ChEs and *h*CAs. The synthesized compounds also showed high inhibitory effects on ChEs and *h*CA isoenzymes. In particular, newly developed derivatives exhibited higher inhibitory activity than reference compounds. When the results were analyzed, it was revealed that the R1 and R2 variants in the pyrazole carboxamide structure caused a change in the inhibition activity on these enzymes. The results of *in vitro* and *in vivo* studies have been shown to support each other and the binding affinities of the strongest inhibitors at the active sites of target enzymes. The observed differences in activity and selectivity between derivatives are attributed to structural differences with unique steric and binding properties. In this study, it is thought that this enzyme-specific inhibitor design will contribute to the development of alternative potential agents that can be used in the treatment of diseases such as glaucoma and AD.

Funding

This work was supported by the Research Fund of Anadolu University (grant number 2102 S003).

Author Contributions

Conceptualization, M.D., and M.I.; Methodology, M.D., S.A., N.L., F.T., Ü.M.K., C.T., M.I., and Ş.B.; Validation, C.T.; Formal analysis, M.D., S.A., N.L., F.T., Ü.M.K., C.T., M.I.; Writing, M.D., M.I., and C.T.; Funding acquisition, Ş.B. All authors have read and agreed to the published version of the manuscript.

Conflict of Interests

The authors declare no conflict of interest.

Data Availability Statement

The data that support the findings of this study are available from the corresponding author upon reasonable request.

Keywords: Pyrazole carboxamide · carbonic anhydrase inhibitors · glaucoma · cholinesterase inhibitors · molecular docking

[1] C. T. Supuran, *Nat. Rev. Drug Discovery* **2008**, *7*, 168–181.
[2] S. B. Ceyhun, M. Şentürk, E. Yerlikaya, O. Erdoğan, Ö. İ. Küfrevioğlu, D. Ekinci, *Environ. Toxicol. Pharmacol.* **2011**, *32*, 69–74.
[3] C. T. Supuran, *Clin. Sci.* **2021**, *135*, 1233–1249.
[4] F. Carta, L. Di Cesare Mannelli, M. Pinard, C. Ghelardini, A. Scozzafava, R. McKenna, C. T. Supuran, *Bioorg. Med. Chem.* **2015**, *23*, 1828–1840.
[5] V. M. Krishnamurthy, G. K. Kaufman, A. R. Urbach, I. Gitlin, K. L. Gudiksen, D. B. Weibel, G. M. Whitesides, *Chem. Rev. (Washington, DC, U.S.)* **2008**, *108*, 946–1051.
[6] C. T. Supuran, *Expert Opin. Ther. Pat.* **2018**, *28*, 709–712.
[7] S. Akocak, Ö. Güzel-Akdemir, R. Kishore Kumar Sanku, S. S. Russom, B. I. Iorga, C. T. Supuran, M. A. Ilies, *Bioorg. Chem.* **2020**, *103*, 104204.
[8] J. T. Andring, M. Fouch, S. Akocak, A. Angeli, C. T. Supuran, M. A. Ilies, R. McKenna, *J. Med. Chem.* **2020**, *63*, 13064–13075.
[9] C. T. Supuran, *Future Med. Chem.* **2021**, *13*, 1935–1937.
[10] C. T. Supuran, A. Scozzafava, *Bioorg. Med. Chem.* **2007**, *15*, 4336–4350.
[11] M. Aggarwal, R. McKenna, *Expert Opin. Ther. Pat.* **2012**, *22*, 903–915.
[12] P. C. McDonald, M. Swayampakula, S. Dedhar, *Metabolites* **2018**, *8*, 20.
[13] M. F. Sugrue, *Prog. Ret. Eye Res.* **2000**, *19*, 87–112.
[14] R. Ulus, M. Kaya, D. Demir, E. Tunca, M. Bülbül, *J. Enzyme Inhib. Med. Chem.* **2016**, *31*, 63–69.
[15] M. O. Gordon, M. A. Kass, *Arch. Ophthalmol.* **1999**, *117*, 573–583.
[16] C. Ward, S. P. Langdon, P. Mullen, A. L. Harris, D. J. Harrison, C. T. Supuran, I. H. Kunkler, *Cancer Treat. Rev.* **2013**, *39*, 171–179.
[17] C. B. Mishra, S. Kumari, A. Angeli, S. Bua, M. Tiwari, C. T. Supuran, *J. Med. Chem.* **2018**, *61*, 3151–3165.
[18] A. Kumar, K. Siwach, C. T. Supuran, P. K. Sharma, *Bioorg. Chem.* **2022**, *126*, 105920.
[19] C. T. Supuran, *Biochem. J.* **2016**, *473*, 2023–2032.
[20] V. Alterio, A. Di Fiore, K. D'Ambrosio, C. T. Supuran, G. De Simone, *Chem. Rev. (Washington, DC, U.S.)* **2012**, *112*, 4421–4468.
[21] C. T. Supuran, V. Alterio, A. Di Fiore, K. D'Ambrosio, F. Carta, S. M. Monti, G. De Simone, *Med. Res. Rev.* **2018**, *38*, 1799–1836.
[22] Q. Istrefi, C. Türkeş, M. Arslan, Y. Demir, A. R. Nixha, Ş. Beydemir, Ö. İ. Küfrevioğlu, *Arch. Pharm. (Weinheim, Ger.)* **2020**, *353*, 1900383.
[23] A. L. Collins, T. J. Aitken, V. Y. Greenfield, S. B. Ostlund, K. M. Wassum, *Neuropsychopharmacol.* **2016**, *41*, 2830–2838.
[24] L. M. T.-G. Ruivo, K. L. Baker, M. W. Conway, P. J. Kinsley, G. Gilmour, K. G. Phillips, J. T. Isaac, J. P. Lowry, J. R. Mellor, *Cell Rep.* **2017**, *18*, 905–917.
[25] G. Provensi, M. B. Passani, A. Costa, I. Izquierdo, P. Blandina, *Br. J. Pharmacol.* **2020**, *177*, 557–569.
[26] C. D. Benham, T. B. Bolton, R. J. Lang, *Nature* **1985**, *316*, 345–347.
[27] P. T. Francis, *CNS Spect.* **2005**, *10*, 6–9.
[28] İ. Gülçin, A. Scozzafava, C. T. Supuran, Z. Koksal, F. Turkan, S. Çetinkaya, Z. Bingöl, Z. Huyut, S. H. Alwasel, *J. Enzyme Inhib. Med. Chem.* **2016**, *31*, 1698–1702.
[29] S. Shenhar-Tsarfaty, S. Berliner, N. M. Bornstein, H. Soreq, *J. Mol. Neurosci.* **2014**, *53*, 298–305.
[30] H. Zhang, Y. Wang, Y. Wang, X. Li, S. Wang, Z. Wang, *Eur. J. Med. Chem.* **2022**, *240*.
[31] R. Krieger, Ed. *Hayes' handbook of pesticide toxicology*; 3rd ed., Vol. 1, San Dieogp: Academic Press, **2010**, pp. 1908.
[32] M. Reale, E. Costantini, M. Di Nicola, C. D'Angelo, S. Franchi, M. D'Aurora, M. Di Bari, V. Orlando, S. Galizia, S. Ruggieri, et al., *Sci. Rep.* **2018**, *8*, 1319.
[33] H. Gao, Y. Jiang, J. Zhan, Y. Sun, *Bioorg. Chem.* **2021**, *114*, 105149.
[34] P. Kessler, P. Marchot, M. Silva, D. Servent, *J. Neurochem.* **2017**, *142*, 7–18.
[35] M. Işık, Ş. Beydemir, *Arch. Physiol. Biochem.* **2022**, *128*, 352–359.
[36] A. Katić, V. Kašuba, N. Kopjar, B. T. Lovaković, A. M. Marjanović Čermak, G. Mendaš, V. Micek, M. Milić, I. Pavičić, A. Pizent, et al., *Chem.-Biol. Interact.* **2021**, *338*, 109287.
[37] G. M. Chuiko, *Comp. Biochem. Physiol. C Toxicol. Pharmacol.* **2000**, *127*, 233–242.
[38] M. Singh, M. Kaur, H. Kukreja, R. Chugh, O. Silakari, D. Singh, *Eur. J. Med. Chem.* **2013**, *70*, 165–188.
[39] G. D. Stanciu, A. Luca, R. N. Rusu, V. Bild, S. I. Beschea Chiriac, C. Solcan, W. Bild, D. C. Ababei, *Biomolecules* **2019**, *10*, 40 .
[40] W. T. Chiu, T. Y. Lee, L. Chan, D. Wu, L. K. Huang, D. Y.T. Chen, Y. T. Lee, C. J. Hu, C. T. Hong, *Clin. Neuro. Neurosurg.* **2020**, *195*, 105959.
[41] M. Işık, *Neurochem. Res.* **2019**, *44*, 2147–2155 .
[42] M. Zaman, A. N. Khan, Wahiduzzaman, S. M. Zakariya, R. H. Khan, *Int. J. Biol. Macromol.* **2019**, *134*, 1022–1037.
[43] L. S. Schneider, *Dialog. Clin. Neurosci.* **2000**, *2*, 111–128 .
[44] R. R. Gupta, M. Kumar, V. Gupta, *Heterocyclic Chemistry: Volume II: Five-Membered Heterocycles*; Springer Science & Business Media, **2013**.
[45] J. J. Li, *Knorr pyrazole synthesis, In Name Reactions: A Collection of Detailed Reaction Mechanisms*, Li, J. J., Ed.; Springer Berlin Heidelberg: Berlin, Heidelberg, **2006**, pp. 331–334.
[46] A. Ansari, A. Ali, M. Asif, *New J. Chem.* **2017**, *41*, 16–41 .
[47] S. Fustero, M. Sánchez-Roselló, P. Barrio, A. Simón-Fuentes, *Chem. Rev. (Washington, DC, U.S.)* **2011**, *111*, 6984–7034.
[48] C. Yamali, H. Sakagami, K. Satoh, K. Bandow, Y. Uesawa, S. Bua, A. Angeli, C. T. Supuran, H. I. Gul, *Bioorg. Chem.* **2022**, *127*, 105969.
[49] C. Yamali, H. Sakagami, Y. Uesawa, K. Kurosaki, K. Satoh, Y. Masuda, S. Yokose, A. Ece, S. Bua, A. Angeli, C. T. Supuran, *Eur. J. Med. Chem.* **2021**, *217*, 113351.
[50] G. Steinbach, P. M. Lynch, R. K. S. Phillips, M. H. Wallace, E. Hawk, G. B. Gordon, N. Wakabayashi, B. Saunders, Y. Shen, T. Fujimura, et al, *N. Engl. J. Med.* **2000**, *342*, 1946–1952 .
[51] G. Li, Y. Cheng, C. Han, C. Song, N. Huang, Y. Du, *RSC Med. Chem.* **2022**, *13*, 1300–1321 .
[52] E. Cullen, *J. Pharm. Sci.* **1984**, *73*, 579–589.
[53] C. Hampp, A. G. Hartzema, T. L. Kauf, *Value Health* **2008**, *11*, 389–399.
[54] K. Tsutomu, N. Toshitaka, *Neuropharmacology* **1978**, *17*, 249–256.
[55] J. García-Lozano, J. Server-Carrió, E. Escrivà, J.-V. Folgado, C. Molla, L. Lezama, *Polyhedron* **1997**, *16*, 939–944.
[56] I. M. Spitz, B. H. Novis, R. Ebert, S. Trestian, D. LeRoith, W. Creutzfeldt, *Metabolism* **1982**, *31*, 380–382.
[57] D. Luttinger, D. J. Hlasta, *Chapter 3 Antidepressant Agents. In Annu. Rep. Med. Chem.*, Bailey, D. M., Ed.; Academic Press, **1987**, Volume 22, pp. 21–30.
[58] E. Olah, M. S. Lui, D. Y. Tzeng, G. Weber, *Cancer Res.* **1980**, *40*, 2869–2875.
[59] P. G. Canonico, P. B. Jahrling, W. L. Pannier, *Antiviral Res.* **1982**, *2*, 331–337 .
[60] P. Taslimi, K. Turhan, F. Türkan, H. S. Karaman, Z. Turgut, I. Gulcin, *Bioorg. Chem.* **2020**, *97*, 103647.
[61] F. Turkan, A. Cetin, P. Taslimi, İ. Gulçin, *Arch. Pharm. (Weinheim, Ger.)* **2018**, *351(10)*, 1800200.
[62] C. Türkeş, S. Akocak, M. Işık, N. Lolak, P. Taslimi, M. Durgun, İ. Gulçin, Y. Budak, Ş. Beydemir, *J. Biomol. Struct. Dyn.* **2022**, *40(19)*, 8752-8764.
[63] N. Lolak, S. Akocak, M. Durgun, H. E. Duran, A. Necip, C. Türkeş, M. Işık, Ş. Beydemir, *Mol. Diversity* **2023**, *27*, 1735–1749.
[64] R. Hron, B. S. Jursic, *Tetrahedron Lett.* **2014**, *55(9)*, 1540-1543.
[65] B. P. Bandgar, S. S. Gawande, R. G. Bodade, N. M. Gawande, C. N. Khobragade, *Bioorg. Med. Chem.* **2009**, *17*, 8168–8173.
[66] P. Taslimi, F. Türkan, A. Cetin, H. Burhan, M. Karaman, I. Bildirici, İ. Gulçin, F. Şen, *Bioorg. Chem.* **2019**, *92*, 103213.
[67] A. Çetin, İ. Bildirici, *J. Saudi Chem. Soc.* **2018**, *22*, 279–296.
[68] F. Turkan, A. Cetin, P. Taslimi, M. Karaman, İ. Gulçin, *Bioorg. Chem.* **2019**, *86*, 420–427.
[69] Y. Dizdaroglu, C. Albay, T. Arslan, A. Ece, E. A. Turkoglu, A. Efe, M. Senturk, C. T. Supuran, D. Ekinci, *J. Enzyme Inhib. Med. Chem.* **2020**, *35*, 289–297.
[70] H. H. Li, C. Wu, S. L. Zhang, J. G. Yang, H. L. Qin, W. Tang, *J. Enzyme Inhib. Med. Chem.* **2022**, *37(1)*, 2099-2111.
[71] A. Benazzouz-Touami, A. Chouh, S. Halit, S. Terrachet-Bouaziz, M. Makhloufi-Chebli, K. Ighil-Ahriz, A. M. Silva, *J. Mol. Struct.* **2022**, *1249*, 131591.
[72] Z. Zhang, J. Min, M. Chen, X. Jiang, Y. Xu, H. Qin, W. Tang, *Eur. J. Med. Chem.* **2020**, *201*.
[73] G. L. Qiu, S. S. He, S. C. Chen, B. Li, H. H. Wu, J. Zhang, W. J. Tang, *J. Enzyme Inhib. Med. Chem.* **2018**, *33(1)*, 1506-1515.
[74] M. W. Duffel, I. S. Ing, T. M. Segarra, J. A. Dixson, C. F. Barfknecht, R. D. Schoenwald, *J. Med. Chem.* **1986**, *29*, 1488–1494 .
[75] M. al-Rashida, S. Hussain, M. Hamayoun, A. Altaf, J. Iqbal, *Biomed Res. Int.* **2014**, *2014*, 162928.
[76] C. Yamali, H. I. Gul, M. Tugrak Sakarya, B. Nurpelin Saglik, A. Ece, G. Demirel, M. Nenni, S. Levent, A. Cihat Oner, *Bioorg. Chem.* **2022**, *124*, 105822.

[77] K. V. Dileep, K. Ihara, C. Mishima-Tsumagari, M. Kukimoto-Niino, M. Yonemochi, K. Hanada, M. Shirouzu, K. Y. J. Zhang, *Int. J. Biol. Macromol.* **2022**, *210*, 172–181.
[78] F. Nachon, E. Carletti, C. Ronco, M. Trovaslet, Y. Nicolet, L. Jean, P.-Y. Renard, *Biochem. J.* **2013**, *453*, 393–399 .
[79] S. Chakravarty, K. K. Kannan, *J. Mol. Biol.* **1994**, *243*, 298–309.
[80] K. H. Sippel, A. H. Robbins, J. Domsic, C. Genis, M. Agbandje-McKenna, R. McKenna, *Acta Crystallogr. Sect. F Struct. Biol. Cryst. Commun.* **2009**, *65*, 992–995 .
[81] G. L. Ellman, K. D. Courtney, V. Andres, R. M. Featherstone, *Biochem. Pharmacol.* **1961**, *7*, 88–95.
[82] D.-M. Liu, B. Xu, C. Dong, *TrAC, Trends Anal. Chem.* **2021**, *142*, 116320.
[83] Ü. M. Koçyiğit, P. Taslimi, B. Tüzün, H. Yakan, H. Muğlu, E. Güzel, *J. Biomol. Struct. Dyn.* **2022**, *40*, 4429–4439.
[84] M. Wang, X. Gu, G. Zhang, D. Zhang, D. Zhu, *Anal. Chem.* **2009**, *81*, 4444–4449 .
[85] J. A. Verpoorte, S. Mehta, J. T. Edsall, *J. Biol. Chem.* **1967**, *242*, 4221–4229 .
[86] J. M. Armstrong, D. V. Myers, J. A. Verpoorte, J. T. Edsall, *J. Biol. Chem.* **1966**, *241*, 5137–5149 .
[87] N. Lolak, S. Akocak, C. Türkeş, P. Taslimi, M. Işık, Ş. Beydemir, İ. Gülçin, M. Durgun, *Bioorg. Chem.* **2020**, *100*, 103897.
[88] K. A. Johnson, R. S. Goody, *Biochem.* **2011**, *50*, 8264–8269 .
[89] T. C. Chou, P. Talalay, *J. Biol. Chem.* **1977**, *252*, 6438–6442.
[90] H. Lineweaver, D. Burk, *J. Am. Chem. Soc.* **1934**, *56*, 658–666 .
[91] J.-M. G. Rodriguez, N. P. Hux, S. J. Philips, M. H. Towns, *J. Chem. Educ.* **2019**, *96*, 1833–1845.
[92] Schrödinger Release 2023–2: Protein Preparation Wizard, Schrödinger, LLC, New York, NY, 2023.
[93] Schrödinger Release 2023–2: LigPrep, Schrödinger, LLC, New York, NY, 2023.
[94] C. Lu, C. Wu, D. Ghoreishi, W. Chen, L. Wang, W. Damm, G. A. Ross, M. K. Dahlgren, E. Russell, C. D. Von Bargen, et al., *J. Chem. Theory Comput.* **2021**, *17*, 4291–4300.
[95] Schrödinger Release 2023–2: Epik, Schrödinger, LLC, New York, NY, 2023.
[96] J. C. Shelley, A. Cholleti, L. L. Frye, J. R. Greenwood, M. R. Timlin, M. Uchimaya, *J. Comput.-Aided Mol. Des.* **2007**, *21*, 681–691 .
[97] Schrödinger Release 2023–2: Receptor Grid Generation, Schrödinger, LLC, New York, NY, 2023.
[98] G. Yapar, H. E. Duran, N. Lolak, S. Akocak, C. Türkeş, M. Durgun, M. Işık, Ş. Beydemir, *Bioorg. Chem.* **2021**, *117*, 105473.
[99] Ö. Güleç, C. Türkeş, M. Arslan, Y. Demir, B. Dincer, A. Ece, Ş. Beydemir, *J. Biomol. Struct. Dyn.* **2023**, 1–19.
[100] Schrödinger Release 2023–2: SiteMap, Schrödinger, LLC, New York, NY, 2023.
[101] Schrödinger Release 2023–2: Glide, Schrödinger, LLC, New York, NY, 2023.
[102] A. Buza, C. Türkeş, M. Arslan, Y. Demir, B. Dincer, A. R. Nixha, Ş. Beydemir, *Int. J. Biol. Macromol.* **2023**, *239*, 124232.
[103] R. A. Friesner, J. L. Banks, R. B. Murphy, T. A. Halgren, J. J. Klicic, D. T. Mainz, M. P. Repasky, E. H. Knoll, M. Shelley, J. K. Perry, et al. *J. Med. Chem.* **2004**, *47*, 1739–1749 .
[104] T. A. Halgren, R. B. Murphy, R. A. Friesner, H. S. Beard, L. L. Frye, W. T. Pollard, J. L. Banks, *J. Med. Chem.* **2004**, *47*, 1750–1759 .
[105] A. Daina, O. Michielin, V. Zoete, *Sci. Rep.* **2017**, *7*, 42717 .

Manuscript received: November 15, 2023
Accepted manuscript online: December 27, 2023
Version of record online: January 22, 2024